Chemical Science

ROYAL SOCIETY OF CHEMISTRY

PERSPECTIVE

View Article Online
View Journal | View Issue

Cite this: *Chem. Sci.*, 2020, **11**, 5614

All publication charges for this article have been paid for by the Royal Society of Chemistry

Peptide and protein modified metal clusters for cancer diagnostics

Dongdong Su, [a] Liang Gao, [a] Fuping Gao, [b] Xiangchun Zhang[c] and Xueyun Gao *[a]

The biomedical features of metal clusters have been explored in tumor diagnostic applications in recent years. Peptide or protein protected metal clusters with low toxicity, ultra-small size and good biocompatibility are ideal bioanalytical tools, and exhibit better cancer diagnostic properties that have been attractive to oncologists. This perspective provides a rigorous but succinct overview of cancer diagnosis as a working concept for metal clusters by reporting the latest significant advances in the applications of metal clusters in tumor-related bioanalysis and diagnosis. The materials design principles, bioanalytical mechanisms and biomedical applications of metal clusters are described, and then the potential challenges and prospects of metal clusters in cancer diagnosis are discussed. A perspective addressing the role of metal clusters in this field is required to understand their effects and functions, as well as for the scientific community to further advance the development of metal clusters for broader diagnostic applications.

Received 28th February 2020
Accepted 7th May 2020

DOI: 10.1039/d0sc01201g

rsc.li/chemical-science

1. Introduction

Early accurate cancer diagnosis has attracted widespread public attention and is the first imperative issue in the treatment of cancer.[1] On the other hand, traditional clinical diagnostic methods, including body fluid testing, pathological tissue testing and clinical image testing, rely on different reagents and instruments, as well as different data analysis standards. This causes a potential problem, that is, various test data have different evaluation standards, and it is difficult to achieve the normalization of the data system. Therefore, there is an urgent need to develop rapid, specific and sensitive agents and methods for cancer diagnosis. Nanobiotechnology, especially the use of metal clusters with biological and biomedical effects

[a]Department of Chemistry and Chemical Engineering, Beijing University of Technology, Beijing 100124, China. E-mail: gaoxy@ihep.ac.cn
[b]Institute of High Energy Physics, Chinese Academy of Sciences, Beijing 100049, China
[c]Tea Research Institute, Chinese Academy of Agricultural Sciences, Hangzhou, 310008, China

*Dongdong Su received his Master's degree in organic chemistry from Nankai University in 2010 and PhD degree in 2014 from the National University of Singapore under the supervision of Prof. Young-Tae Chang. After postdoctoral research in Prof. Young-Tae Chang's group at the Singapore Bioimaging Consortium, A*Star (2014–2018), he worked at Beijing University of Technology as an associate professor. His research focuses on the development of smart molecular probes/nanoprobes and combined imaging technologies for tumor diagnostics and treatment.*

Liang Gao received her PhD in physical chemistry from the Institute of Chemistry, Chinese Academy of Sciences in 2012. She is now an associate professor at Beijing University of Technology. One of her research interests focuses on exploring a highly sensitive and selective method for analyzing cell membrane proteins in situ, both in vitro and in vivo. The analytical method as-established is expected to facilitate the assessment of the clinical stage of malignant cancer patients and screen optimal treatments. She is also expected to develop a potential molecular targeted agent to improve the therapeutic effect of fatal diseases, such as malignant tumors.

for the diagnosis of diseases, is an emerging and active research area.[2,3] The above problems can be solved by using metal clusters for disease diagnosis. Metal clusters use unified data processing standards in multi-dimensional diagnosis and detection of body fluids, cells and tissues. The unity of data standards can significantly improve the accuracy and consistency of diagnosis. At the same time, metal clusters exhibit much improved biocompatibility and renal clearance characteristics, which offers a great opportunity for advancing the fields of bioanalysis, diagnosis and nanomedicine.[4,5]

Metal clusters, especially gold and silver clusters, possess fascinating optical, magnetic and electronic properties, and are the most promising ultra-small nanomaterials with potential applications benefiting from their ultra-small size and clear molecular structures. The need for detecting and labelling important biological analytes has driven considerable research efforts in developing metal clusters in catalysis, biosensing and fluorescent bioimaging applications, which gained rapid development and are widely evaluated.[6–9] However, limited efforts have been made for metal clusters in the diagnostic applications. Thanks to advances in mass spectrometry technology, a great deal of effort has been invested to synthesize metal clusters with precise atomic numbers.[10] Compared to metal nanoparticles, atomically precise metal clusters show significantly different optical features and molecular purities.[11] The molecular composition of these types of metal clusters is characterized by a well-defined molecular formula, such as the precise number of metal atoms and ligands, which can be effectively used for accurate detection analysis and mass spectroscopic imaging analysis, and can be further used for fundamental research and development of wider diagnostic applications.[12] Furthermore, recent studies have shown that gold clusters have been used as radiosensitizers for cancer radiotherapy and as effective antimicrobial agents for killing bacteria, benefiting from their therapeutic effects.[13,14] The growing popularity of metal clusters has been realized in the fields of biomedical applications.

Proteins and peptides have very good biocompatibility and have been widely used in biological applications. At the same time, certain specific structures of biomolecules also have specific disease models or organ targeting capabilities, enabling them to act as ligands for metal clusters and serve as functional biological targeting molecules.[15,16] The integration of metal clusters with biomolecules can have a synergistic effect on the physicochemical and physiological properties of metal clusters, combining the unique optical and electronic properties of metal clusters with the biological functions of biomolecules. Moreover, by controlling the synthesis conditions by using various biomolecules, changes in size and surface modifications can also be achieved, which can better meet the diagnosis needs of different diseases.

The need for improved integration of accurate disease detection, as well as the practical considerations for clinical transformable nanomaterials, will be key drivers of diagnostics in the near future. In this perspective, we aim to provide a brief overview of metal clusters for tumor diagnosis, including the preparation and characterization of peptide/protein modified metal clusters and their applications in tumor-related bioanalysis and cancer diagnosis (Fig. 1). The current challenges

Fuping Gao received her PhD (2008) in biomedical engineering from the Chinese Academy of Medical Sciences & Peking Union Medical College. From 2008 to 2010, she worked as a postdoctoral researcher in Tsinghua University. She now works as an associate professor at the Key Laboratory for the Biological Effects of Nanomaterials and Nanosafety, Institute of High Energy Physics, Chinese Academy of Sciences. Her research interests focus on the biomedical effects of nanomaterials.

Xiangchun Zhang received his PhD in bioinorganic chemistry from the Institute of High Energy Physics, Chinese Academy of Sciences in 2019. He is now an assistant professor at the Tea Research Institute, Chinese Academy of Agricultural Sciences. His research focuses on the design, synthesis, separation and purification of metal clusters and their application in tumor metastasis.

Xueyun Gao received his PhD in physics from the Institute of Solid State Physics, Chinese Academy of Sciences in 2003. From 2003 to 2007, he did his postdoctoral work in bionanotechnology with Prof. Hiroshi Matsui at Hunter College. In 2007, he started his academic career at the Institute of High Energy Physics, Chinese Academy of Sciences. In 2017, he moved to Beijing University of Technology as a professor. His research interests are in the development of bioprobes for in vitro/vivo cancer biomarker detection and metal clusters for clinical diagnosis and therapy.

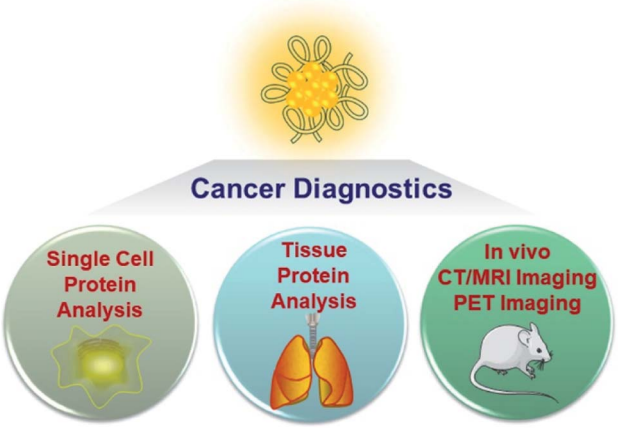

Fig. 1 Schematic illustration of the cancer diagnosis applications of metal clusters in this perspective.

and prospects of peptide/protein modified metal clusters for cancer diagnosis will also be provided. We expect that this perspective will promote a deeper understanding of metal clusters in cancer diagnosis and facilitate the discovery of new types of cancer diagnostics.

2. Fabrication and characterization of peptide/protein modified metal clusters

Thiol-protected metal clusters are ultra-small nanomaterials stabilized by thiol ligands. Glutathione (GSH), peptides or proteins are commonly used as a thiol donor to prepare metal clusters for biodiagnosis. Briefly, the structure of metal clusters consists of two parts: a metal core and a ligand shell. The biomacromolecular thiol donor of the organic shell used in the synthesis is functionalized to stabilize and regulate the formation of metal clusters, thereby forming a highly stable metal system. At the same time, high purity and stable repeatable synthetic methods allow for accurate characterization. Peptide and protein modified metal clusters can help maintain the biological activity of peptides and proteins after cluster formation. By analyzing the structure of metal clusters, we can understand the role of metal clusters in life activities, such as the effect of size on optical behavior and disease diagnosis in organisms, further promoting the applications of these new materials in cancer diagnosis.

2.1 Design of peptide modified metal clusters

The evolution of peptide modified metal clusters and their optical properties has aroused great interest for their biomedical applications. In the presence of thiols, the chemical reduction of Au(III) ions is a common tendency to synthesize such clusters. GSH, a tripeptide consisting of glycine, cysteine, and glutamic acid, was first used to protect stable gold clusters by Schaaff's group.[17] Using $NaBH_4$ as a reducing agent, Au was reduced in medium to synthesize Au clusters, and the final product was defined as $Au_{28}(GSH)_{16}$ based on ESI-MS analysis. Furthermore, the size of Au clusters can be controlled by changing the mixture of solvents. Xie *et al.* developed another strategy for synthesizing GSH protected Au clusters by heating a mixture of $HAuCl_4$ and GSH solutions at 70 °C for 24 h.[18] Here, GSH is used both as a template for metal cluster synthesis and as a reducing agent. Since then, a number of new methods have been developed for the synthesis of atomically precise metal clusters.[19,20]

Inspired by the stable synthesis of atomically precise metal clusters and potential biological applications, the synthesis of metal clusters using peptides as templates has gradually flourished. Peptides with specific amino acid sequences play a pivotal role in the preparation of metal clusters for biomedical applications. Several special advantages of peptides and the design principles of peptide-modified metal clusters are as follows: (1) peptides have good biocompatibility and enhance their prospects in biological applications; (2) certain thiol-containing specific amino acids have good metal ion reduction and coordination ability to form uniform and stable metal clusters, such as cysteine (C) and methionine, tyrosine (Y) and tryptophan; (3) designed specific peptide sequences have the ability to achieve targeting functions for molecules, antigens and cancer model tissues.[21] By introducing the above amino acid fragments and targeting functional peptide sequences, we can rationally design peptide-protected metal clusters with different targeting capabilities. Meanwhile, by optimizing the synthesis conditions, we can construct functional metal clusters with different structures, sizes and charges for biomedical applications.

2.2 Design of protein modified metal clusters

Proteins, owing to their good biocompatibility and biological functions, have also been used in metal cluster preparations and have shown potential biological applications. Xie *et al.* reported a simple one-pot synthesis procedure under mild reaction conditions termed as protein-directed synthesis, which can be used as an ideal platform for preparing protein-protected metal clusters. Briefly, a solution of $HAuCl_4$ and bovine serum albumin (BSA) was vigorously stirred at 37 °C for a short period of time, and then the pH of the solution was adjusted to 12, which can activate the reducing ability of BSA to form Au clusters *in situ*.[22] Similarly, in this synthesis approach, proteins serve as the synthesis templates, as well as reducing agents for metal ions. Using similar synthetic procedures, different commercially available proteins have been used to synthesize protein modified metal clusters, such as lysozyme,[23,24] lactoferrin,[25] trypsin,[26] pepsin,[27] insulin[28] and peroxidase.[29]

Among all these types of protein modified metal clusters, both metal cores and protein shells contribute to their physicochemical properties. Protein modified metal clusters with desirable properties have been successfully prepared with high compatibility and preserved bioactivity. Several special advantages of proteins and the design principles of protein-modified metal clusters are as follows: (1) metal atoms encapsulated in proteins not only produce fluorescence, but also obtain good

steric protection from bulky protein molecules, endowing the metal clusters with high stability that facilitates their applications *in vitro* and *in vivo*; (2) the capability to maintain the biological activity of the protein after cluster formation due to mild conditions and ultrasmall size that limit the conformational changes of the protein; (3) the protein molecule usually contains free amino or carboxyl groups that can be used for further modifications, such as antibodies or prodrugs, thereby expanding the range of applications of metal clusters in biological systems.

3. Tumor diagnosis with metal clusters

3.1 Quantitative analysis of tumor biomarkers in single cells

Changes in the expression of specific proteins in cells can serve as important signals for cancer or other disease states. Through accurate proteomic analysis of specific cells, deep understanding of the role of cellular heterogeneity in disease progression can be achieved, which is of great significance for the early diagnosis of diseases.[30] Therefore, how to achieve sensitive and accurate quantitative analysis of specific proteins at the single cell level has always been one of the directions of chemical biologists. Although some methods have been developed to quantify single-cell protein, their quantitative accuracy is still limited, and the method is very time consuming and cumbersome.[31] Reliable and effective single-cell protein quantitative analysis is urgent to develop for the early diagnosis of cancer. Mass spectrometry (MS) technology provides acceptable capabilities in protein analysis; especially, laser ablation inductively coupled plasma mass spectrometry (LA-ICPMS) allows high spatial resolution (higher than 1 μm) and well-resolved MS signals and images of the specimen can be obtained in rather short time.[32] Metal clusters with a specific targeting peptide and precise atomic numbers combined with LA-ICPMS can accurately identify and quantify specific proteins of individual cells by targeting peptide functions and accurately calculating metal content.[32,33]

Using this approach, there have been some examples of single cell protein quantification *in situ*. Peptide-modified Au clusters have enabled accurate quantification of $\alpha_{IIb}\beta_3$ on single human erythroleukemia (HEL) cells.[34] The expression level of integrin $\alpha_{IIb}\beta_3$ was found to be associated with blood coagulation and cancer progression, such as invasion and metastasis of human melanoma cells and prostate cancer and HEL cells.[35–37] To this end, the peptide H_2NCCYKKKKQAGDV-COOH (abbreviated as CV) was designed, in which CCY has the ability to capture Au clusters and the portion of KQAGDV has specificity for integrin $\alpha_{IIb}\beta_3$.[37] The prepared peptide–Au clusters emitted red fluorescence (647 nm) and the precise molecular composition ($Au_{24}CV_8$) was determined by matrix-assisted laser desorption/ionization-time of flight mass spectrometry (MALDI-TOF-MS). After confirming the specificity of the $\alpha_{IIb}\beta_3$ target by fluorescence imaging, $Au_{24}CV_8$ achieved successful and accurate observation of integrin $\alpha_{IIb}\beta_3$ at the single cell level. In the meantime, benefiting from cytofluorolabeling and solution-based LA-ICPMS techniques, the average amount of $\alpha_{IIb}\beta_3$ on an individual HEL cell was quantified by calculating the average mass of Au on a single cell, showing that the expression level of integrin $\alpha_{IIb}\beta_3$ on a single HEL cell ranged from 5.75×10^{-17} to 9.11×10^{-17} mol (Fig. 2).[34]

More metal clusters with precise atomic numbers have been developed for the quantitative analysis of different tumor biomarkers. Using the novel and versatile approach described above, a new type of Au cluster was further reported to accurately quantify protein expression levels in three tumor cell lines,[38] wherein the peptide YHWYGYTPQNVI portion functioned as a specific target sequence of the epidermal growth factor receptor (EGFR) of the cell membrane.[39] The probe composition was defined by MALDI-TOF-MS as Au_5Peptide$_3$, and its fluorescence characteristics were used for cell membrane EGFR imaging by confocal microscopy. Thanks to the accurate formula and specific targeting capabilities of the probe, EGFR expression levels in SMMC-7721, KB and HeLa cells were successfully quantified at the single cell level and distinguished in these cell lines.

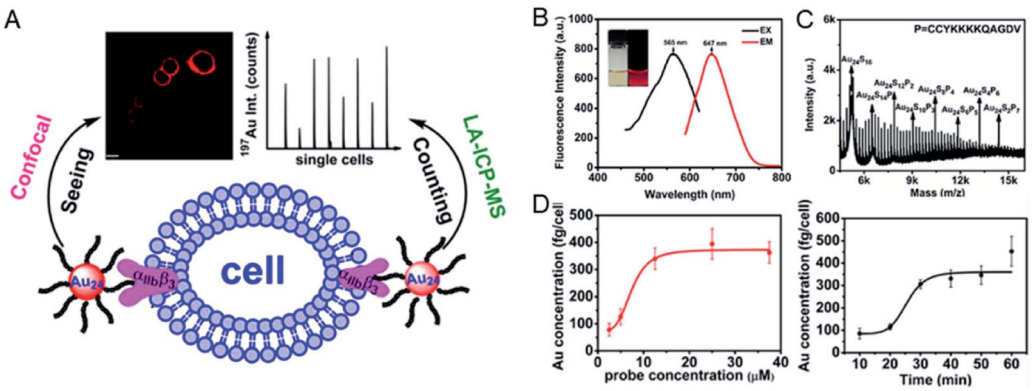

Fig. 2 (A) Schematic illustration of the quantitative detection of $\alpha_{IIb}\beta_3$ on a single cell by using metal clusters. (B) Photoexcitation and photoemission spectra of the probe. (C) MALDI-TOF-MS spectra of the probe. (D) The mean mass of Au per cell (left) and the time-dependent incubation results (probe concentration: 12.5 μM; right). Reproduced from ref. 34 with permission from the American Chemical Society, copyright 2015.

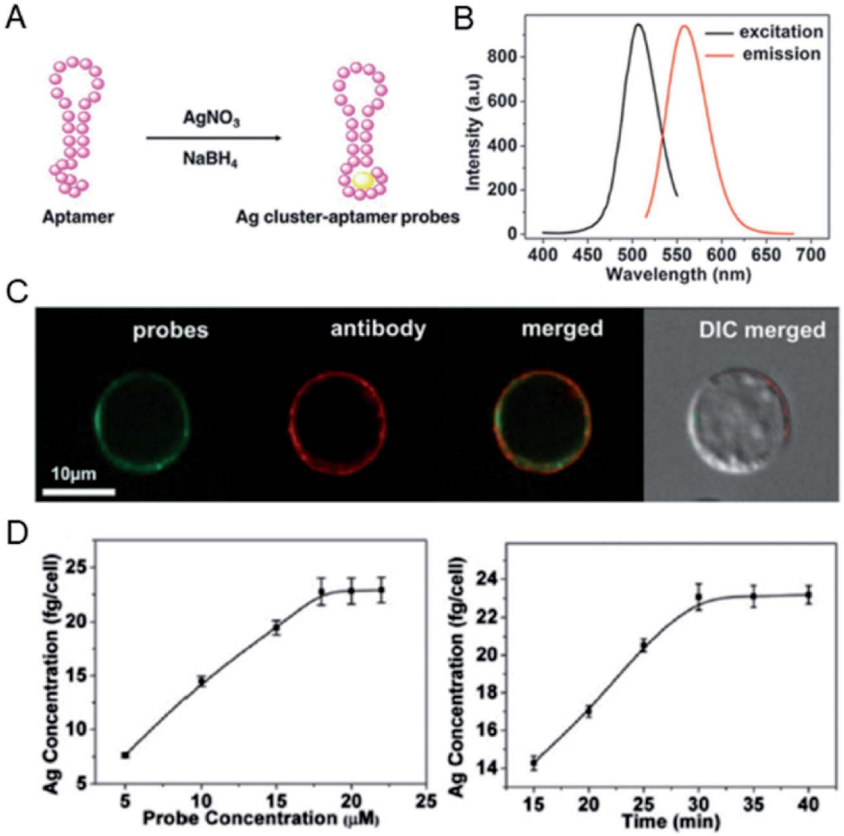

Fig. 3 (A) Preparation of a Ag cluster–aptamer. (B) Fluorescence spectra of the probe. (C) Confocal imaging of the Ag cluster–aptamer and *anti*-mIgM in Ramos cells. (D) The relationship between probe concentration and the Ag concentration of the labeled cell (left); the concentration-dependent incubation results (probe concentration: 20 mM; right). Reproduced from ref. 40 with permission from the Royal Society of Chemistry, copyright 2014.

In addition to Au clusters, silver clusters are also used to quantify tumor biomarkers at the single cell level. Ag clusters constructed from specific aptamers can provide fluorescent imaging information as well as accurate spatial and mass information of mIgM in living cells.[40] In this case, Ag clusters were constructed using a cytosine-modified TD05.1 sequence aptamer named TDC05.1.[41] Under optimized conditions, the fluorescence of the probe was used to accurately label mIgM in Ramos cells and co-localize well with the antibody. Furthermore, quantification of the amount of mIgM present on a single Ramos cell was achieved by calculating the Ag number using ICP-MS. The amount of mIgM in a single cell was determined to be 7.10×10^{-7} mol per cell, which is consistent with the data determined by the ELISA standard curve (Fig. 3).

Due to the diversity of metal clusters, they can specifically target the corresponding proteins in the cell membrane, and can label and quantify the versatile proteins in cells. This analytical approach can be further extended to simultaneously quantify multiple proteins in different invasive tumor cell lines. The expression levels of membrane type-1 matrix metalloproteinase (MT1-MMP) and integrin $\alpha_v\beta_3$ protein on the cell membrane determine the invasive ability of tumor cells and are key to tumorigenesis, metastasis and prognosis.[42,43] The use of different metal clusters enables high sensitivity and accurate quantification of the expression levels of MT1-MMP and integrin $\alpha_v\beta_3$, thereby precisely distinguishing tumor cells with different invasive capabilities. In this study, red-emitting Au clusters (P1–Au) and green-emitting Ag clusters (P2–Ag) with two functional peptides were constructed. Specific visualization and targeting of MT1-MMP and integrin $\alpha_v\beta_3$ on the cell membrane were realized by the prepared P1–Au clusters and P2–Ag clusters. Then MT1-MMP and integrin $\alpha_v\beta_3$ can be accurately quantified by calculating the Au or Ag content in the same single cell.[44] Under optimized conditions, P1–Au and P2–Ag clusters can simultaneously target and label the two different proteins specifically in the same single cell, and further analyze the invasive capacity of SiHa and HeLa cells at the same single cell by analyzing the Au/Ag signals for MT1-MMP/integrin $\alpha_v\beta_3$ *via* LA-ICPMS (Fig. 4). The results showed that the expression levels of MT1-MMP and integrin $\alpha_v\beta_3$ were higher in SiHa cells than in HeLa cells, revealing individual differences in the invasive ability of the same tumor cell line.

3.2 Quantitative analysis of biomarkers in tissues

After demonstrating their ability to quantify proteins in single cells, metal clusters were also used to quantify the expression levels of primary tumor-specific biomarkers in tissues.[32] Quantifying primary tumor-specific biomarkers and thus accurately

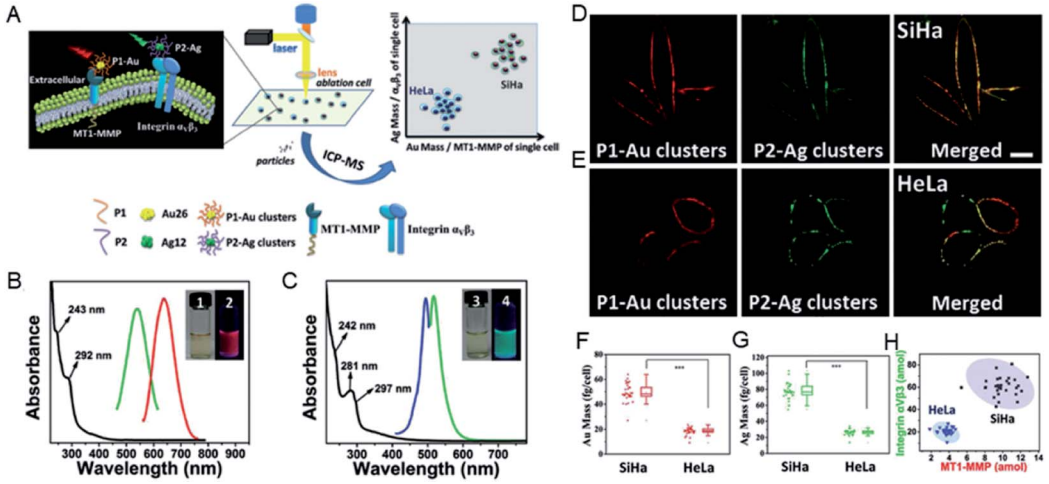

Fig. 4 (A) Scheme of the quantitative differentiation for invasive capacity of SiHa and HeLa cell populations. (B) Spectral information of P1–Au clusters and (C) P2–Ag clusters. (D and E) CLSM images of mixed clusters in SiHa and HeLa cells (probe concentration: 9×10^{-6} M). (F and G) The mass plots of Au and Ag on SiHa and HeLa cells. (H) 2D mass plots on SiHa (black) and HeLa (blue) cell lines. Reproduced from ref. 44 with permission from Wiley-VCH Verlag GmbH & Co. KGaA, Weinheim, copyright 2018.

diagnosing tumor invasion and metastasis play a key role in early cancer therapy, and have never been achieved through current pathologic studies. Peptide-modified Au clusters with a specific mass signal can be applied to quantify the levels of MT1-MMP in primary tumor tissues to accurately assess the risk of primary tumor invasion and metastasis (Fig. 5).[45] In detail, the expression levels of MT1-MMP in human lung adenocarcinoma PC-14 and A549 cells were evaluated based on the results of LA-ICPMS, and the results demonstrated that MT1-MMP was more expressed in PC-14 cells. Further analysis showed that the expression level of MT1-MMP was correlated with the invasion and metastasis rate of lung adenocarcinoma cells. Due to the precise atomic number of Au clusters, the quantitative analysis of MT1-MMP in PC-14 and A549 xenograft tissues can be achieved and visualized by 2D-LA-Mass mapping. In addition, this method was further used to assess real clinical tissues. The 2D-LA-Mass mapping method was applied to observe and quantify the expression level of MT1-MMP in primary human lung carcinoma and human renal carcinoma tissue sections, and accurately assess the risk of primary tumor invasion and metastasis.[45]

In addition, precise metal clusters can also be used as elemental labels to provide signal amplification in LA-ICPMS bioimaging. The Fernandez group reported a sensitive methodology to quantitatively determine metallothioneins (MT 1/2 protein isoforms) in human retina tissue sections by LA-ICPMS.[46] Au clusters are used as a label to provide a high amplification, which allowed conversion of 2D quantitative images of the distribution of MT 1/2 in the neurosensory retina layers by LA-ICPMS. The results were complementary to those determined using commercial ELISA kits (Fig. 6). Later, by conjugating water-soluble Au clusters with an antibody, immunoassays for MT 1/2 and MT 3 in the retina of ocular tissue sections were performed using fluorescence confocal microscopy and LA-ICPMS. The authors used the same method to visualize the distribution of MT 1/2 and MT 3 in human ocular tissue.[47] In 2019, the same group released a new application of Au clusters using LA-ICPMS to simultaneously quantitatively image Fe and ferroportin (FPN) in the hippocampus CA1 region of brain tissues from Alzheimer's disease (AD) patients and healthy controls (HCs) (Fig. 7).[48] The results showed elevated Fe concentrations in AD patients compared to HCs, while concentrations of FPN in AD patients were similar compared to those in HCs. This format was further extended to other metal clusters, such as Ag or Pt.[49,50] Similar gold clusters have also been developed as chemical tongue sensor arrays for Alzheimer's disease.[51]

In short, abnormal changes in the number of specific proteins are significantly associated with the development and progression of the disease. The combination of metal clusters with precise atomic numbers and mass spectrometry provides a simple and accurate way to quantify the identifiable target proteins and helps estimate the protein function and accurately assess the dynamic progression of tumor cells in early tumor diagnosis. The applications of metal clusters in tumor cells and real clinical tissue samples will provide guidance for the clinical diagnostic and prognosis of patients with primary tumors.

3.3 Metal clusters for CT/MRI imaging

So far, the bioimaging applications of metal clusters are mainly based on their fluorescent properties.[7,52] In recent years, computed tomography (CT) has been used as one of the most powerful and widely used noninvasive clinical diagnostic tools.[53] Au has a higher atomic number ($Z = 79$) than iodine ($Z = 53$), and is used in contrast agents for CT. Metal clusters may have longer circulation times and better biocompatibility. At the same time, the physical size (<5 nm) gives metal clusters the potential for use as CT imaging contrast agents. An emerging body of research is beginning to use Au as a CT agent.[54–56] Examples of Au clusters for CT imaging of cancer were reported

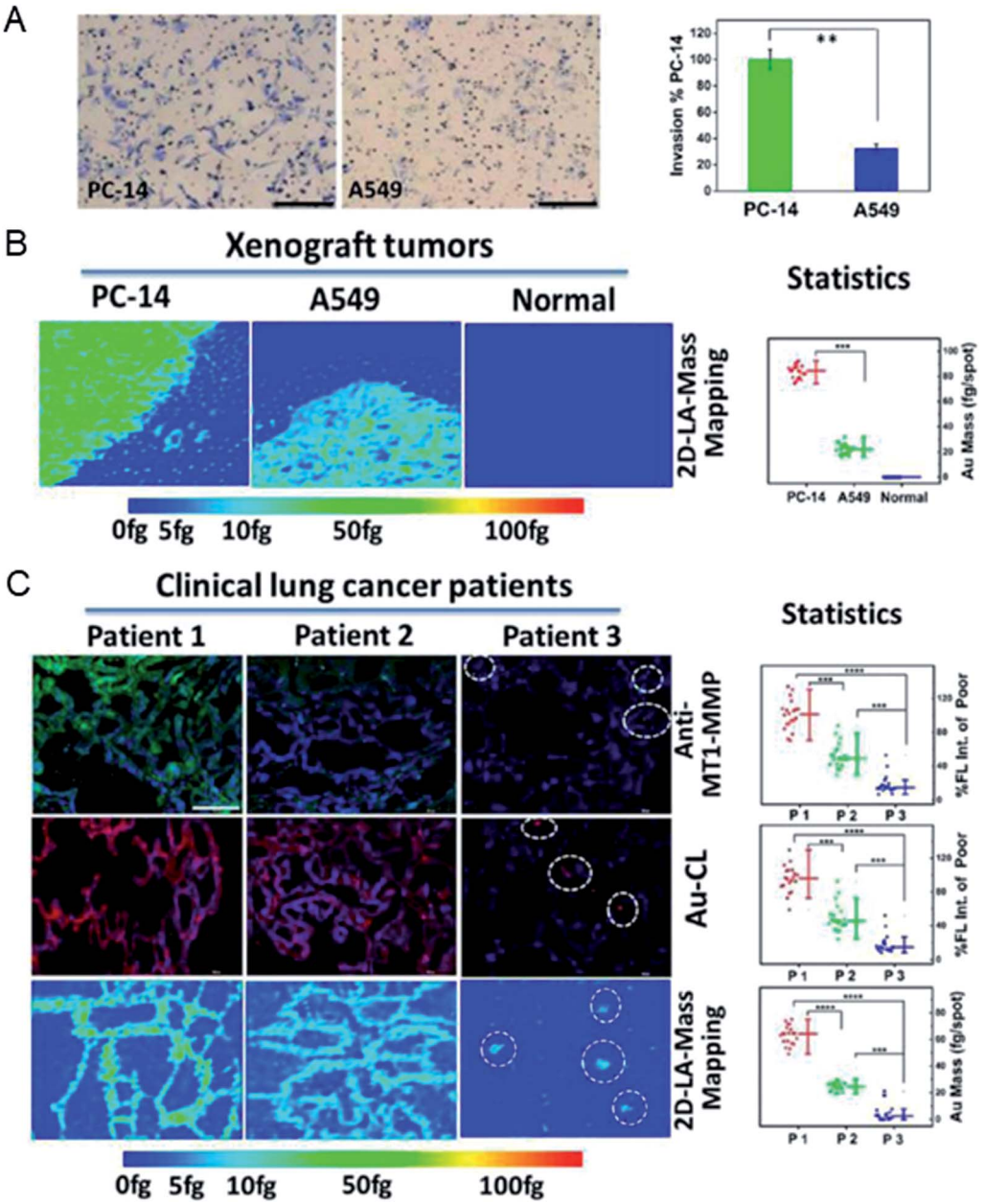

Fig. 5 (A) Invasion images of PC-14 cells and A549 cells *in vitro*. (B) Analysis of MT1-MMP in xenograft tumor tissue sections by 2D-LA-Mass mapping. (C) Analysis of MT1-MMP in clinical lung tumor tissues. Reproduced from ref. 45 with permission from the American Chemical Society, copyright 2018.

to be dual CT/optical imaging probes with target molecule specificity for cancer imaging.[57] Blum *et al.* developed a new class of activity-based probes (ABPs) that target cathepsin for functional CT imaging of cancer. The results showed that the detection of CT contrast from tumors is inversely related to the size of gold nanoparticles and the amount of targeting moiety.[58] Protein modified gold clusters have also been studied as CT agents in the same period. In 2011, Zheng *et al.* studied CT imaging of GSH-protected Au clusters in order to observe the urinary excretion of these Au clusters in real time within 24 hours after IV injection into mice (Fig. 8). The results showed that GSH protected Au clusters can be effectively eliminated from the body, and evidence suggests that only 3.7% of Au clusters accumulate in the liver and more than 50% are found in urine.[59] Their ultra-small size and low affinity to serum proteins minimize the accumulation of clusters in the liver and spleen, reducing the background of CT imaging. Zhang *et al.* also reported Au clusters as contrast agents for CT enhanced imaging.[60] The good characteristics of gold clusters themselves and the results of these studies encourage the future use of gold clusters as CT reagents.

Gao's group developed BSA protected Au clusters for the detailed CT imaging of the kidneys. After optimizing the ratio of BSA to Au, the prepared clusters emitted 645 nm fluorescence

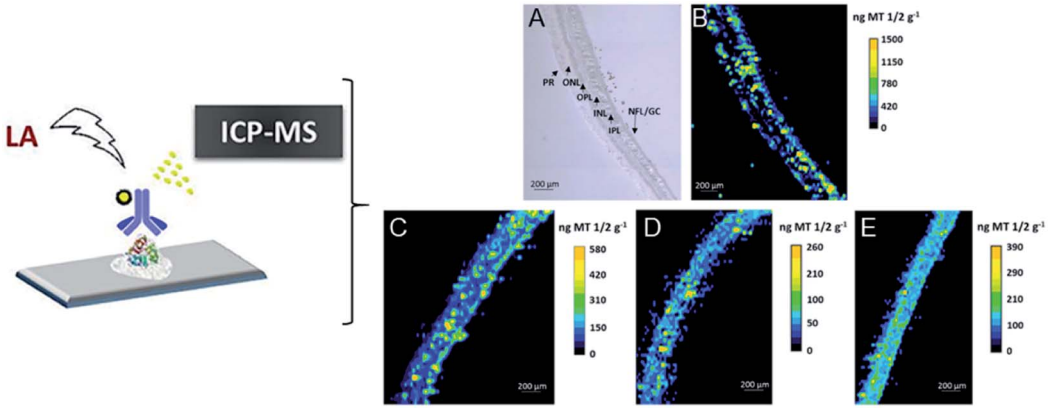

Fig. 6 Distribution images of MT 1/2 in the human retina by LA-ICPMS. (A) TEM for the analyzed retina layers from donor 1; (B) image of donor 1 by LA-ICPMS; (C) image of donor 2; (D) image of donor 3; (E) image of donor 4. Reproduced from ref. 46 with permission from the American Chemical Society, copyright 2018.

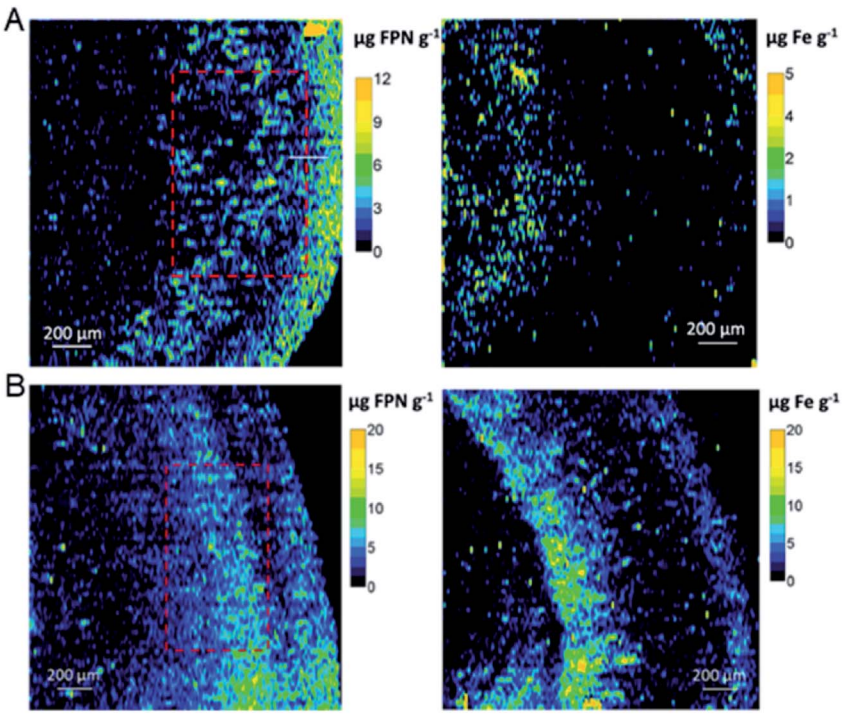

Fig. 7 Quantitative images for FPN and Fe by LA-ICPMS from the hippocampus CA1 region of human brain tissues. (A) HC human brain. (B) AD patient brain. Reproduced from ref. 48 with permission from Elsevier, copyright 2019.

and showed enhanced X-ray attenuation. *In vitro* CT images of Au clusters showed that at the same concentration, the HU value of BSA–Au is much higher than that of iopromide. *In vivo* studies have shown that Au clusters are distributed in the liver, spleen and kidneys, and are excreted mainly by the kidneys. Under optimal conditions, the agent can successfully outline the anatomical structure of mouse kidneys by using 2D and 3D computed tomography imaging techniques, and the renal collection system and ureters are clearly visible (Fig. 9).[61] The application of these label-free BSA–Au clusters demonstrates that metal clusters are suitable for CT diagnosis, and further CT diagnostic applications are still being explored.

Later, Chen's group reported a method for preparing dual-modality fluorescence/CT iodinated gold clusters (AuNCs@BSA-I) using BSA and chloramine-T for accurate diagnosis of thyroid cancer (Fig. 10).[62] *In vitro* imaging of AuNCs@BSA-I showed a strong fluorescent signal and similar X-ray attenuation to iopamidol, which are suitable for *in vivo* CT imaging. *In vivo* CT imaging showed that the clusters are easy to concentrate in thyroid tissue and can accurately and selectively diagnose malignant thyroid cancer.

In addition to CT imaging, magnetic resonance imaging (MRI) is also one of the important techniques for clinic diagnosis of diseases. It has the advantages of high resolution and

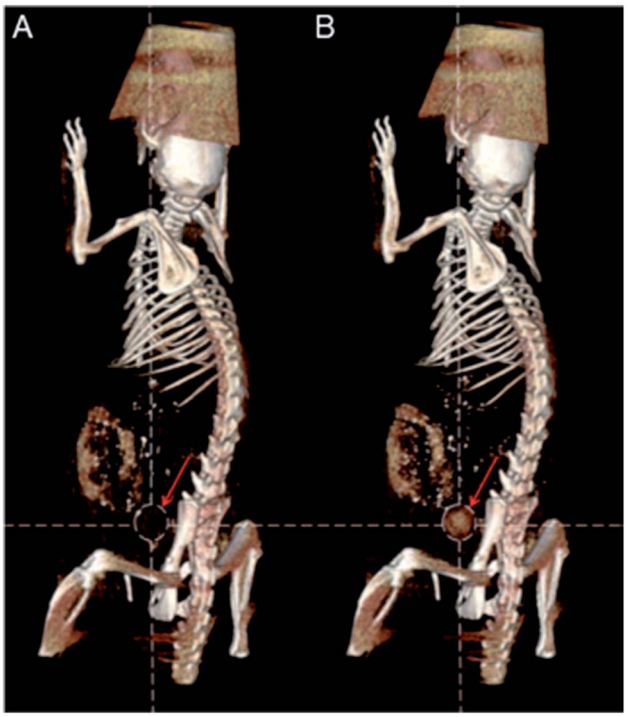

Fig. 8 (A) CT images before injection. (B) CT images at 30 min after IV injection of GS-AuNPs. Reproduced from ref. 59 with permission from Wiley-VCH Verlag GmbH & Co. KGaA, Weinheim, copyright 2011.

deeper tissue penetration.[63] In order to obtain more complementary information from different types of imaging modalities, it is important to develop hybrid metal clusters for multimodal imaging for accurate diagnosis of tumors, which can recompense the drawbacks of each single imaging modality.[64]

In 2013, Cai's group prepared BSA protected hybrid gold–gadolinium clusters for trimodal fluorescence/CT/MRI imaging.[65] The prepared hybrid clusters have ultrasmall size, good stability and perfect biocompatibility, and *in vivo* performance was demonstrated through fluorescence imaging, CT and MRI, respectively (Fig. 11). Experiments have shown that after intravenous injection, the hybrid nanoclusters can effectively accumulate in tumor sites and rapidly clear through renal excretion, indicating they have the ability of tumor targeting and a low background from body residues. In addition, the clusters can penetrate solid tumors through effective tumor targeting, and do not cause potential toxicity in the body.

3.4 Metal clusters for PET imaging

Positron emission tomography (PET) possesses high-dimensional quantitative features that provide quantitative support for decisions surrounding cancer detection.[66,67] Radiolabeled metal clusters have been developed for PET imaging and have revealed improved radiolabel stability and diagnostic accuracy. ^{64}Cu is an ideal radioisotope with a half-life of 12.7 h

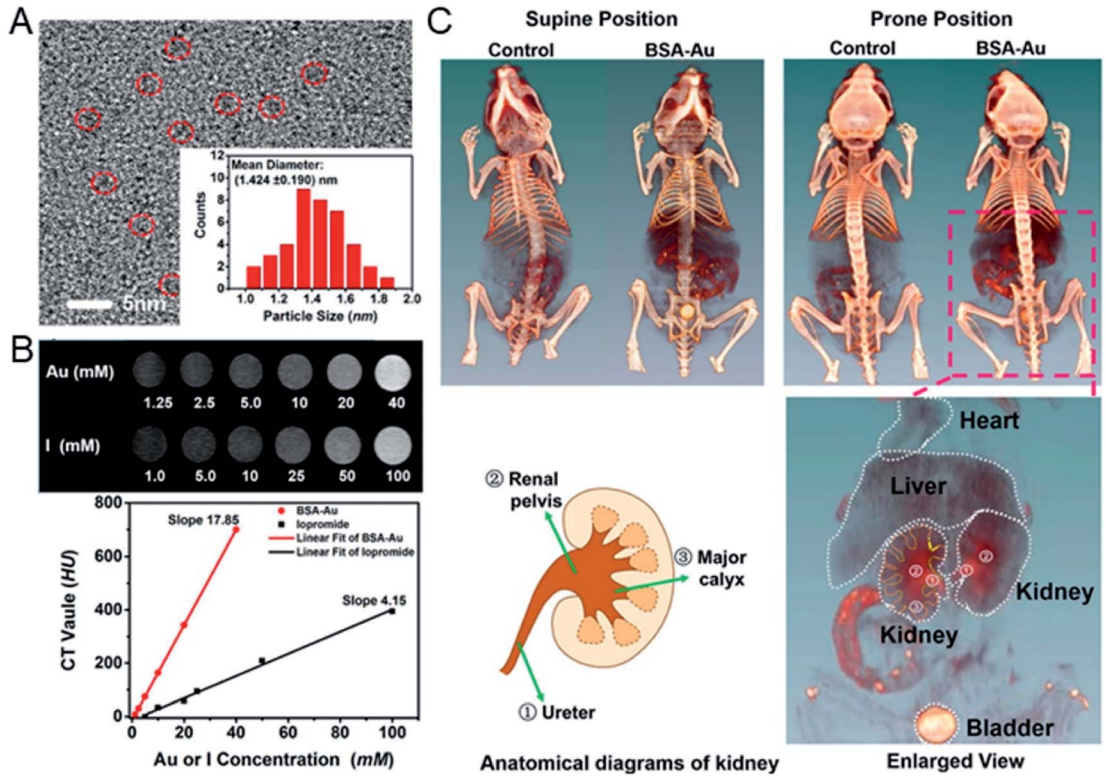

Fig. 9 (A) HRTEM image of BSA–Au clusters and the size distribution of the Au cluster. (B) *In vitro* comparison of CT images and HU values of BSA–Au clusters and the iopromide solution. (C) *In vivo* 3D CT images of control and BSA–Au cluster-injected mice at 2 h post injection. Reproduced from ref. 61 with permission from the American Chemical Society, copyright 2015.

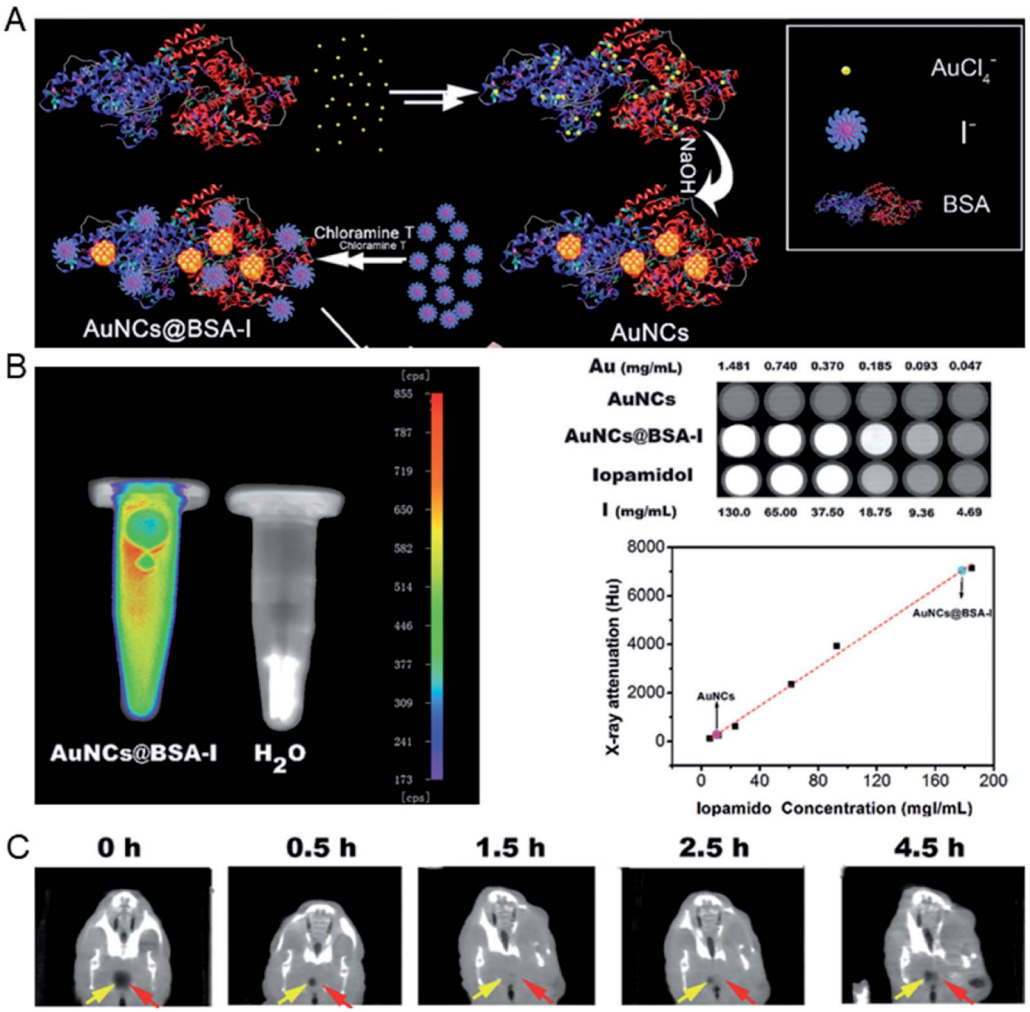

Fig. 10 (A) Schematic illustration of the preparation of AuNCs@BSA-I. (B) *In vitro* fluorescence and CT images of AuNCs@BSA-I and evaluation of the radiopacity of AuNCs@BSA-I with Iopamidol as a reference. (C) *In vivo* CT imaging of an orthotopic thyroid cancer mouse injected with AuNCs@BSA-I. Reproduced from ref. 62 with permission from the Royal Society of Chemistry, copyright 2017.

and decay characteristics (β^+, 0.653 MeV, 17.8%; β^-, 0.579 MeV, 38.4%) for PET imaging and has been used for cancer diagnosis.[68,69] In recent years, simple and general chelator-free ^{64}Cu-integrated Au nanomaterials (NMs) for PET imaging have been developed by reducing ^{64}Cu(II) on the surface of PEG-stabilized Au NMs, such as spherical Au nanoparticles, Au nanorods and Au nanohexapods. Then the accurate and sensitive localization of ^{64}Cu-integrated Au NMs can be monitored and quantitatively analyzed using noninvasive PET imaging.[70] Different types of chelator-free ^{64}Cu radiolabeled materials were evaluated, such as ^{64}Cu–AuNPs with different surface coatings using embedded ^{64}Cu,[71] [^{64}Cu]CuInS/ZnS QDs through incorporating ^{64}Cu into the CuInS/ZnS structure,[72] ^{64}Cu-labeled lipid nanocapsules,[73] and so on. However, these types of materials possess relatively large particle size and cause biotoxicity due to their significant liver accumulation and slow clearance *in vivo*.

Peptide or protein protected Cu clusters with ultrasmall size may have better imaging performance *in vivo*. For example, the [^{64}Cu]Cu clusters constructed using BSA as a template were developed as an ultra-small chelator-free radioactive ^{64}Cu PET agent for the diagnosis of orthotopic lung tumors (Fig. 12).[74] In the ultra-small [^{64}Cu]Cu clusters, ^{64}Cu was an integral building block of clusters rather than chelated to the clusters; therefore its radiolabeling stability was greatly improved, which can avoid the problem of misunderstanding PET imaging results due to the false signal generated by isolated ^{64}Cu from the agent. At the same time, a lung tumor target peptide (luteinizing hormone releasing hormone, LHRH) can be first introduced into BSA molecules to achieve better targeting properties. The prepared [^{64}Cu]Cu clusters ([^{64}Cu]CuNC@BSA-LHRH) exhibited high radiolabel stability and ultra-small size, which facilitated renal clearance. After intravenous injection, [^{64}Cu]Cu clusters showed rapid spread to the target orthotopic tumor in the left lung, while the PET imaging background in the right lung and other organs was negligible. The importance of this research work is that Cu clusters act as a stable PET agent, providing high-resolution and high-sensitivity diagnosis for orthotopic tumors while allowing the detection of small-sized malignancies at much lower radiation doses.

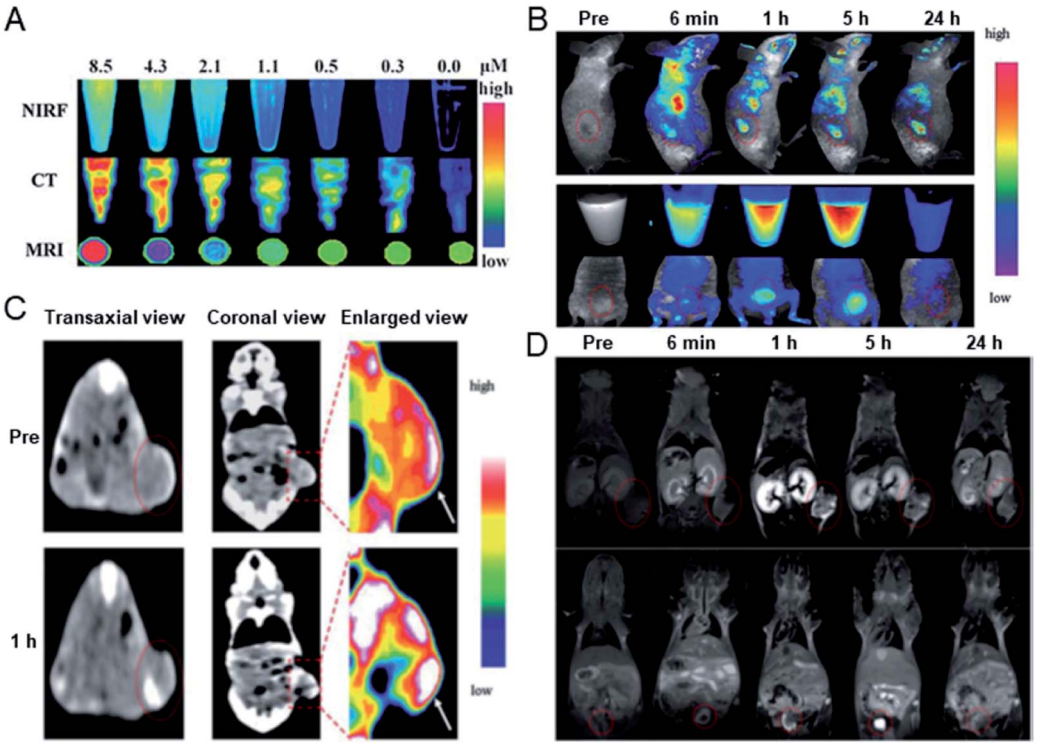

Fig. 11 (A) Fluorescence/CT/MRI trimodal imaging of hybrid gold–gadolinium clusters. (B) *In vivo* fluorescence imaging of mice after the injection of metal clusters. (C) *In vivo* CT and (D) MRI images of mice injected with metal clusters, respectively. Reproduced from ref. 65 with permission from the Royal Society of Chemistry, copyright 2013.

In addition to the preparation of radiolabeled single metal clusters, PET metal cluster imaging agents have also been constructed in an integrated strategy. In 2014, Liu *et al.* reported the process of preparing ^{64}Cu alloyed gold clusters (^{64}CuAuNCs) for PET imaging in a prostate cancer model. The facile synthesis developed in this report allows for the precise control of ^{64}Cu alloy gold clusters for high radiolabel efficiency and stability for sensitive and accurate diagnosis of cancer.[75] Later, ^{64}CuAuNCs-PEG350 was obtained by surface modification with polyethylene glycol (PEG), which showed low mononuclear phagocytic system (MPS) accumulation, together with significant renal and hepatobiliary clearance.[76] The *in vivo* targeting and clearance, pharmacokinetics, and PET imaging capabilities of the new radiolabeled metal clusters were carefully evaluated. *In vivo* PET/CT imaging showed a low background and heterogeneous tumor distribution (Fig. 13). The above studies suggest that controlled radiosynthesis of metal clusters may serve as an entry point for broader cancer diagnosis applications using radioactive alloyed metal clusters in preclinical studies.

Almost at the same time, Chen *et al.* reported a novel design of ^{64}Cu-doped chelator-free gold clusters (^{64}Cu-doped Au clusters) for dual-modality PET and self-illuminating NIR imaging based on Cerenkov resonance energy transfer (CRET).[77] The radionuclide ^{64}Cu was introduced into Au clusters by a chelator-free doping method and served as both an energy donor for NIR fluorescence and a probe for PET imaging. The clusters showed high stability, good water dispersibility and solubility *in vitro*, and non-cytotoxicity and good biocompatibility *in vivo*. In

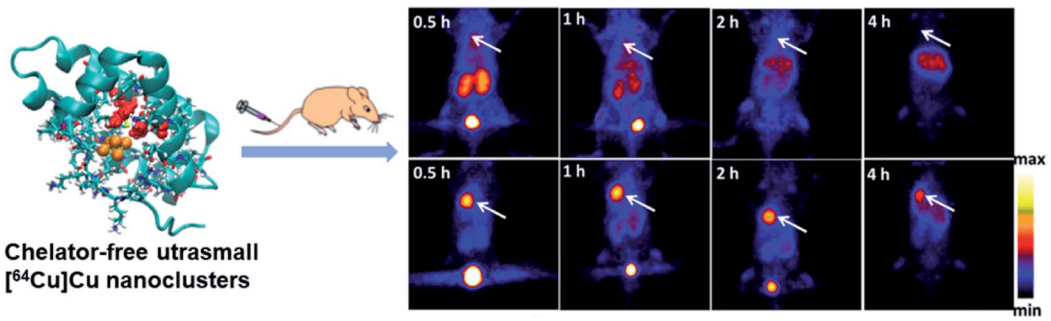

Fig. 12 Comparison of time-dependent PET images of orthotopic A549 lung tumor mice after injection of [^{64}Cu]CuNC@BSA (top) and [^{64}Cu]CuNC@BSA-LHRH (bottom). Reproduced from ref. 74 with permission from the American Chemical Society, copyright 2015.

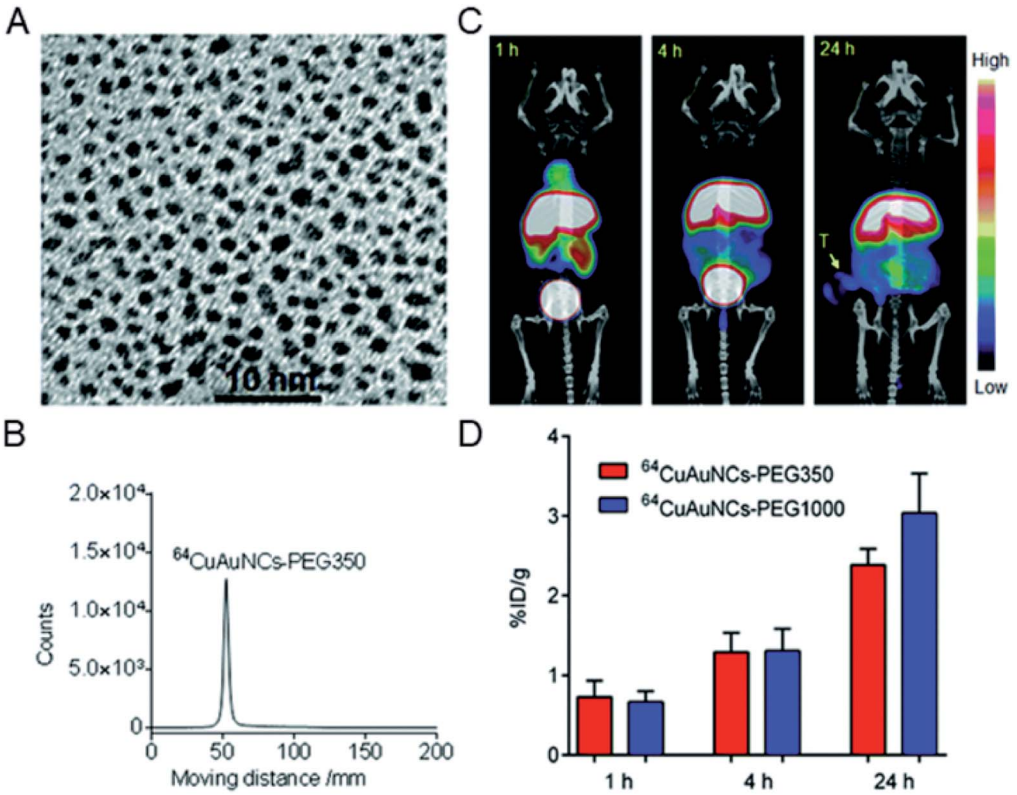

Fig. 13 (A) TEM image of Cu alloyed gold clusters (CuAuNCs). (B) Radio-TLC profile of ^{64}CuAuNCs-PEG350. (C) Representative PET/CT images after injection of ^{64}CuAuNCs-PEG350. (D) Tumor uptake of ^{64}CuAuNCs-PEG350 in PC3 tumor bearing mice. Reproduced from ref. 76 with permission from the Royal Society of Chemistry, copyright 2014.

a U87MG glioblastoma xenograft model, ^{64}Cu-doped Au clusters displayed a high tumor uptake of 15.2% ID per g at 24 h post-injection, and showed effective CRET-NIR imaging and PET imaging both *in vitro* and *in vivo* (Fig. 14A). In 2016, Liu *et al.* reported another ^{64}Cu doped gold cluster. Given that CXCR4 is an up-regulated receptor for primary tumor and lung metastasis, they functionalized the clusters with AMD3100 (or Plerixafor) for PET imaging in an orthotopic breast cancer mouse model (Fig. 14B).[78] The prepared ^{64}CuAuNCs-AMD3100 with a size of 4.5 ± 0.4 nm demonstrated good organ distribution together with significant renal and fecal clearance *in vivo*. PET imaging showed that it enables sensitive and accurate detection of various levels of CXCR4. Importantly, ^{64}CuAuNCs-AMD3100 showed the ability to sensitively detect up-regulated CXCR4 in the early tumors and premetastatic niche of the lungs. The examples of Cu-doped Au clusters provide novel biomedical research tools and new methods for clinical molecular imaging and cancer diagnosis. This is a very important advantage in the potential clinical application of metal clusters.

4. Summary and prospects

Metal clusters have been developed for decades and have been applied for tumor diagnosis *in vivo*. Peptide or protein protected metal clusters are a novel class of metal clusters with precise atomic numbers, ultrasmall size and low toxicity, together with the retained biological activity of the template, which make it possible to use them in a wide range of diagnostic applications. Recent advances in the construction of metal clusters by a variety of peptides or proteins and imaginative approaches have greatly facilitated a basic understanding of their fascinating physical properties and their applications in bioanalysis in the field of cancer diagnosis.

The challenges left by these advances have led us to design and construct metal clusters for many future directions and efforts in tumor diagnosis:

(1) Although peptide or protein protected metal clusters have exhibited the first prospective results in cancer diagnosis, understanding of fundamental structural parameters is still in its early stages and is a challenging issue. Mass spectrometry can provide insight into the ratio of metal to ligand numbers; however, it is still difficult to obtain the exact nature of coordination. Recently, ESI-MS has been demonstrated as a powerful platform to understand the formation mechanism of metal clusters.[79,80] With the development of mass spectrometry technology and the establishment of new detection methods, understanding the formation mechanism of metal clusters protected by a peptide or protein can help better control the stability of clusters around the complicated environment *in vitro* or *in vivo*, and can also help understand the interaction of metal clusters with the biological environment. In practical applications, proteins can be adsorbed and associated with

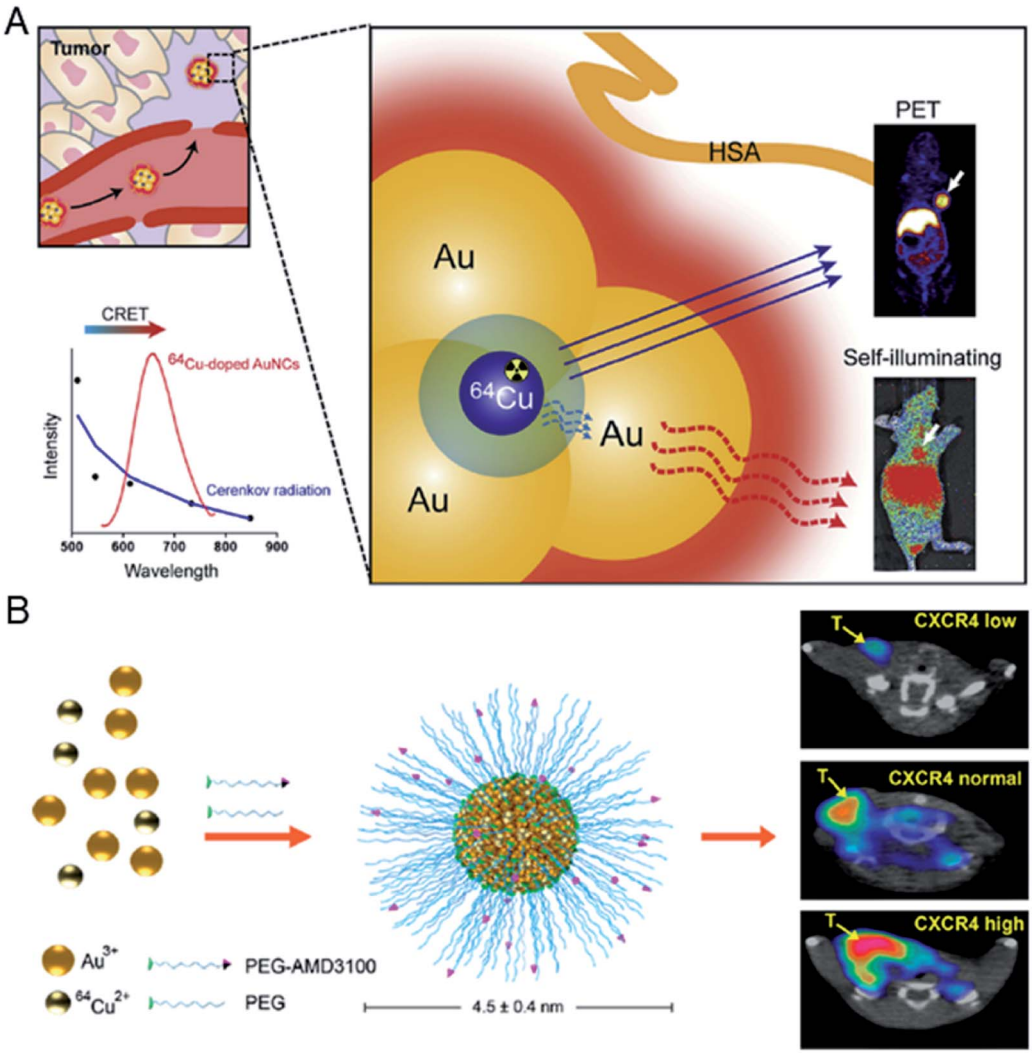

Fig. 14 (A) Schematic illustration of self-illuminating ^{64}Cu-doped gold clusters for self-illuminating NIR images and PET images on mice. Reproduced from ref. 77 with permission from Elsevier, copyright 2014. (B) Schematic illustration of ^{64}CuAuNCs-AMD3100 for PET imaging of CXCR4. Reproduced from ref. 78 with permission from the American Chemical Society, copyright 2016.

clusters, and further research into the biological behavior of proteins and clusters can be conducted, which will further reinforce the insights into their biological functions.

(2) Despite the various advances in reported metal clusters for tumor diagnosis, most of these studies have focused on known functional peptides or limited biomolecules. To offer new discoveries or broaden the application in cancer diagnosis, it is necessary to explore new biomolecule protected metal clusters in order to discover an incredible cancer diagnostic effect in the process, and further exploit in detail the biological properties of metal clusters with minimum side effects.[81] At the same time, the function of metal clusters in disease monitoring can be further explored. A typical example is the use of their intrinsic catalytic activity, such as the enzyme-mimicking activity of metal clusters, which can improve the detection sensitivity and be applied in potential cancer diagnosis.[82,83] For these efforts, researchers can understand the biological properties of metal clusters, such as circulation time, biodistribution, toxicity, and so on. The development and implementation of successful detection will greatly facilitate the accurate diagnosis of early-stage cancer and potentially achieve valuable clinical applications.

(3) In addition to cancer diagnosis, some peptide or protein protected metal clusters have been found to have a therapeutic effect. Recent results show that peptide-modified Au clusters exhibit anticancer effects by targeting and suppressing enzymatic activity in tumor cells, and even achieve therapeutic effects by precisely controlling the size of Au–peptide clusters to inhibit the growth of tumor cells *in vivo*, which provide new concepts and will contribute to the further development of tumor therapy.[84–86] Besides the anti-tumor effect of metal clusters themselves, they have also been used as radiosensitizers in cancer radiotherapy.[87] By using metal clusters as radiosensitizers, a good tumor targeting capability can be achieved while having a high radiotherapy enhancement effect to minimize side effects. In addition, in combination with the imaging

methodology, metal clusters can be used as theranostic agents. These efforts simultaneously endow metal clusters with early diagnosis and rational therapeutic functions. The integration of diagnosis and treatment has also made rapid progress recently. There is an urgent need to achieve synchronous treatment while confirming the accurate diagnosis so as to realize the early diagnosis and treatment of tumors. Further research should focus more on these areas in order to take full advantages of the potential of metal clusters when interested in biomedical applications.

In summary, although metal clusters have made some advances in cancer diagnostic research, the biological application of these clusters is still in its early stages, so there is still much more work to be done before these clusters can be used for true clinical applications, such as thorough toxicity studies, optimization of pharmacokinetic parameters and biodistribution studies that enable the determination of the safety for biomedical applications.[81] With the further advantages of metal clusters design and technological development, we look forward to the widespread application of metal clusters in advanced cancer diagnosis, as well as novel methods for early cancer diagnosis and therapy in future.

Conflicts of interest

There are no conflicts to declare.

Acknowledgements

This work was supported by grants from the National Natural Science Foundation of China (21425522 and 21708029), the Beijing Science and Technology Commission Special Project for Frontier Technology in Life Sciences (No. Z171100000417008) and Beijing Municipal High Level Innovative Team Building Program (IDHT20180504).

Notes and references

1 R. L. Siegel, K. D. Miller and A. Jemal, *Ca-Cancer J. Clin.*, 2018, **68**, 7–30.
2 J. V. Jokerst and S. S. Gambhir, *Acc. Chem. Res.*, 2011, **44**, 1050–1060.
3 P. Cai, W. R. Leow, X. Wang, Y. L. Wu and X. Chen, *Adv. Mater.*, 2017, **29**, 1605529.
4 P. Singh, S. Pandit, V. R. S. S. Mokkapati, A. Garg, V. Ravikumar and I. Mijakovic, *Int. J. Mol. Sci.*, 2018, **19**, 1979.
5 M. X. Yu and J. Zheng, *ACS Nano*, 2015, **9**, 6655–6674.
6 Y. Tao, M. Q. Li, J. S. Ren and X. G. Qu, *Chem. Soc. Rev.*, 2015, **44**, 8636–8663.
7 L. Y. Chen, C. W. Wang, Z. Q. Yuan and H. T. Chang, *Anal. Chem.*, 2015, **87**, 216–229.
8 S. H. Yau, O. Varnavski and T. Goodson, *Acc. Chem. Res.*, 2013, **46**, 1506–1516.
9 H. Liu, G. Hong, Z. Luo, J. Chen, J. Chang, M. Gong, H. He, J. Yang, X. Yuan, L. Li, X. Mu, J. Wang, W. Mi, J. Luo, J. Xie and X.-D. Zhang, *Adv. Mater.*, 2019, **31**, 1901015.
10 I. Chakraborty and T. Pradeep, *Chem. Rev.*, 2017, **117**, 8208–8271.
11 R. Jin, C. Zeng, M. Zhou and Y. Chen, *Chem. Rev.*, 2016, **116**, 10346–10413.
12 C. N. Loynachan, A. P. Soleimany, J. S. Dudani, Y. Y. Lin, A. Najer, A. Bekdemir, Q. Chen, S. N. Bhatia and M. M. Stevens, *Nat. Nanotechnol.*, 2019, **14**, 883–890.
13 X.-D. Zhang, J. Chen, Z. Luo, D. Wu, X. Shen, S.-S. Song, Y.-M. Sun, P.-X. Liu, J. Zhao, S. Huo, S. Fan, F. Fan, X.-J. Liang and J. Xie, *Adv. Healthcare Mater.*, 2014, **3**, 133–141.
14 K. Zheng, M. I. Setyawati, T.-P. Lim, D. T. Leong and J. Xie, *ACS Nano*, 2016, **10**, 7934–7942.
15 Q. Yuan, Y. L. Wang, L. N. Zhao, R. Liu, F. P. Gao, L. Gao and X. Y. Gao, *Nanoscale*, 2016, **8**, 12095–12104.
16 S. L. Deutscher, *Chem. Rev.*, 2010, **110**, 3196–3211.
17 T. G. Schaaff, G. Knight, M. N. Shafigullin, R. F. Borkman and R. L. Whetten, *J. Phys. Chem. B*, 1998, **102**, 10643–10646.
18 Z. T. Luo, X. Yuan, Y. Yu, Q. B. Zhang, D. T. Leong, J. Y. Lee and J. P. Xie, *J. Am. Chem. Soc.*, 2012, **134**, 16662–16670.
19 Y. Gu, Q. Wen, Y. Q. Kuang, L. J. Tang and J. H. Jiang, *RSC Adv.*, 2014, **4**, 13753–13756.
20 Y. L. Wang, Y. Y. Cui, Y. L. Zhao, R. Liu, Z. P. Sun, W. Li and X. Y. Gao, *Chem. Commun.*, 2012, **48**, 871–873.
21 C. L. Charron, J. L. Hickey, T. K. Nsiama, D. R. Cruickshank, W. L. Turnbull and L. G. Luyt, *Nat. Prod. Rep.*, 2016, **33**, 761–800.
22 Z. T. Luo, K. Y. Zheng and J. P. Xie, *Chem. Commun.*, 2014, **50**, 5143–5155.
23 Y. H. Lin and W. L. Tseng, *Anal. Chem.*, 2010, **82**, 9194–9200.
24 H. Wei, Z. D. Wang, L. M. Yang, S. L. Tian, C. J. Hou and Y. Lu, *Analyst*, 2010, **135**, 1406–1410.
25 P. L. Xavier, K. Chaudhari, P. K. Verma, S. K. Pal and T. Pradeep, *Nanoscale*, 2010, **2**, 2769–2776.
26 J. M. Liu, J. T. Chen and X. P. Yan, *Anal. Chem.*, 2013, **85**, 3238–3245.
27 H. Kawasaki, K. Hamaguchi, I. Osaka and R. Arakawa, *Adv. Funct. Mater.*, 2011, **21**, 3508–3515.
28 A. Aires, I. Llarena, M. Moller, J. Castro-Smirnov, J. Cabanillas-Gonzalez and A. L. Cortajarena, *Angew. Chem., Int. Ed.*, 2019, **58**, 6214–6219.
29 F. Wen, Y. Dong, L. Feng, S. Wang, S. Zhang and X. Zhang, *Anal. Chem.*, 2011, **83**, 1193–1196.
30 M. Yu, S. Stott, M. Toner, S. Maheswaran and D. A. Haber, *J. Cell Biol.*, 2011, **192**, 373–382.
31 S. C. Bendall, E. F. Simonds, P. Qiu, A. D. Amir el, P. O. Krutzik, R. Finck, R. V. Bruggner, R. Melamed, A. Trejo, O. I. Ornatsky, R. S. Balderas, S. K. Plevritis, K. Sachs, D. Pe'er, S. D. Tanner and G. P. Nolan, *Science*, 2011, **332**, 687–696.
32 M. Cruz-Alonso, A. Lores-Padin, E. Valencia, H. Gonzalez-Iglesias, B. Fernandez and R. Pereiro, *Anal. Bioanal. Chem.*, 2019, **411**, 549–558.
33 M. Wang, L. N. Zheng, B. Wang, H. Q. Chen, Y. L. Zhao, Z. F. Chai, H. J. Reid, B. L. Sharp and W. Y. Feng, *Anal. Chem.*, 2014, **86**, 10252–10256.

34 J. Zhai, Y. Wang, C. Xu, L. Zheng, M. Wang, W. Feng, L. Gao, L. Zhao, R. Liu, F. Gao, Y. Zhao, Z. Chai and X. Gao, *Anal. Chem.*, 2015, **87**, 2546–2549.
35 S. Kuphal, R. Bauer and A. K. Bosserhoff, *Cancer Metastasis Rev.*, 2005, **24**, 195–222.
36 M. Trikha, J. Timar, S. K. Lundy, K. Szekeres, Y. L. Cai, A. T. Porter and K. V. Honn, *Cancer Res.*, 1997, **57**, 2522–2528.
37 T. A. Springer, J. H. Zhu and T. Xiao, *J. Cell Biol.*, 2008, **182**, 791–800.
38 M. Liu, L. Gao, L. Zhao, J. He, Q. Yuan, P. Zhang, Y. Zhao and X. Gao, *Sci. Rep.*, 2017, **7**, 131.
39 D. Y. An, J. G. Su, J. K. Weber, X. Y. Gao, R. H. Zhou and J. Y. Li, *J. Am. Chem. Soc.*, 2015, **137**, 8412–8418.
40 R. Liu, J. Zhai, L. Liu, Y. Wang, Y. Wei, X. Jiang, L. Gao, H. Zhu, Y. Zhao, Z. Chai and X. Gao, *Chem. Commun.*, 2014, **50**, 3560–3563.
41 P. R. Mallikaratchy, A. Ruggiero, J. R. Gardner, V. Kuryavyi, W. F. Maguire, M. L. Heaney, M. R. McDevitt, D. J. Patel and D. A. Scheinberg, *Nucleic Acids Res.*, 2011, **39**, 2458–2469.
42 M. Tauro, J. McGuire and C. C. Lynch, *Cancer Metastasis Rev.*, 2014, **33**, 1043–1057.
43 J. S. Desgrosellier and D. A. Cheresh, *Nat. Rev. Cancer*, 2010, **10**, 890.
44 X. Zhang, R. Liu, Q. Shu, Q. Yuan, G. Xing and X. Gao, *Small*, 2018, **14**, e1703684.
45 X. C. Zhang, R. Liu, Q. Yuan, F. P. Gao, J. J. Li, Y. Zhang, Y. L. Zhao, Z. F. Chai, L. Gao and X. Y. Gao, *ACS Nano*, 2018, **12**, 11139–11151.
46 M. Cruz-Alonso, B. Fernandez, M. Garcia, H. Gonzalez-Iglesias and R. Pereiro, *Anal. Chem.*, 2018, **90**, 12145–12151.
47 M. Cruz-Alonso, B. Fernandez, L. Alvarez, H. Gonzalez-Iglesias, H. Traub, N. Jakubowski and R. Pereiro, *Mikrochim. Acta*, 2017, **185**, 64.
48 M. Cruz-Alonso, B. Fernandez, A. Navarro, S. Junceda, A. Astudillo and R. Pereiro, *Talanta*, 2019, **197**, 413–421.
49 I. Diez and R. H. Ras, *Nanoscale*, 2011, **3**, 1963–1970.
50 J. Garcia Fernandez, L. Trapiella-Alfonso, J. M. Costa-Fernandez, R. Pereiro and A. Sanz-Medel, *Nanotechnology*, 2015, **26**, 215601.
51 X. Han, Z. Man, S. Xu, L. Cong, Y. Wang, X. Wang, Y. Du, Q. Zhang, S. Tang, Z. Liu and W. Li, *Colloids Surf., B*, 2019, **173**, 478–485.
52 Y. Zheng, L. Lai, W. Liu, H. Jiang and X. Wang, *Adv. Colloid Interface Sci.*, 2017, **242**, 1–16.
53 Y. Iyama, T. Nakaura, M. Kidoh, S. Oda, D. Utsunomiya, N. Sakaino, S. Tokuyasu, H. Osakabe, K. Harada and Y. Yamashita, *Acad. Radiol.*, 2016, **23**, 1393–1401.
54 W. Eck, A. I. Nicholson, H. Zentgraf, W. Semmler and S. Bartling, *Nano Lett.*, 2010, **10**, 2318–2322.
55 J. T. Song, X. Q. Yang, X. S. Zhang, D. M. Yan, Z. Y. Wang and Y. D. Zhao, *ACS Appl. Mater. Interfaces*, 2015, **7**, 17287–17297.
56 D. Kim, Y. Y. Jeong and S. Jon, *ACS Nano*, 2010, **4**, 3689–3696.
57 I. C. Sun, D. K. Eun, H. Koo, C. Y. Ko, H. S. Kim, D. K. Yi, K. Choi, I. C. Kwon, K. Kim and C. H. Ahn, *Angew. Chem., Int. Ed.*, 2011, **50**, 9348–9351.
58 D. Tsvirkun, Y. Ben-Nun, E. Merquiol, I. Zlotver, K. Meir, T. Weiss-Sadan, I. Matok, R. Popovtzer and G. Blum, *J. Am. Chem. Soc.*, 2018, **140**, 12010–12020.
59 C. Zhou, M. Long, Y. P. Qin, X. K. Sun and J. Zheng, *Angew. Chem., Int. Ed.*, 2011, **50**, 3168–3172.
60 A. L. Zhang, Y. Tu, S. B. Qin, Y. Li, J. Y. Zhou, N. Chen, Q. Lu and B. B. Zhang, *J. Colloid Interface Sci.*, 2012, **372**, 239–244.
61 Y. Wang, C. Xu, J. Zhai, F. Gao, R. Liu, L. Gao, Y. Zhao, Z. Chai and X. Gao, *Anal. Chem.*, 2015, **87**, 343–345.
62 X. Chen, H. Zhu, X. Huang, P. Wang, F. Zhang, W. Li, G. Chen and B. Chen, *Nanoscale*, 2017, **9**, 2219–2231.
63 S. Geethanath and J. T. Vaughan, *J. Magn. Reson. Imag.*, 2019, **49**, E65–E77.
64 B. R. Smith and S. S. Gambhir, *Chem. Rev.*, 2017, **117**, 901–986.
65 D. H. Hu, Z. H. Sheng, P. F. Zhang, D. Z. Yang, S. H. Liu, P. Gong, D. Y. Gao, S. T. Fang, Y. F. Ma and L. T. Cai, *Nanoscale*, 2013, **5**, 1624–1628.
66 C. S. Cutler, H. M. Hennkens, N. Sisay, S. Huclier-Markai and S. S. Jurisson, *Chem. Rev.*, 2013, **113**, 858–883.
67 X. Sun, W. Cai and X. Chen, *Acc. Chem. Res.*, 2015, **48**, 286–294.
68 R. Chakravarty, S. Chakraborty and A. Dash, *Mol. Pharm.*, 2016, **13**, 3601–3612.
69 M. Shokeen and C. J. Anderson, *Acc. Chem. Res.*, 2009, **42**, 832–841.
70 X. Sun, X. Huang, X. Yan, Y. Wang, J. Guo, O. Jacobson, D. Liu, L. P. Szajek, W. Zhu, G. Niu, D. O. Kiesewetter, S. Sun and X. Chen, *ACS Nano*, 2014, **8**, 8438–8446.
71 A. F. Frellsen, A. E. Hansen, R. I. Jolck, P. J. Kempen, G. W. Severin, P. H. Rasmussen, A. Kjaer, A. T. Jensen and T. L. Andresen, *ACS Nano*, 2016, **10**, 9887–9898.
72 W. Guo, X. Sun, O. Jacobson, X. Yan, K. Min, A. Srivatsan, G. Niu, D. O. Kiesewetter, J. Chang and X. Chen, *ACS Nano*, 2015, **9**, 488–495.
73 D. S. P. Cai, W. Yang, Z. He, C. Zhang, H. Liu, Z. Liu, X. Zhang, L. Gao, Y. Liu, H. Jiang, F. Gao and X. Gao, *ACS Appl. Bio Mater.*, 2020, **3**, 611–621.
74 F. Gao, P. Cai, W. Yang, J. Xue, L. Gao, R. Liu, Y. Wang, Y. Zhao, X. He, L. Zhao, G. Huang, F. Wu, Y. Zhao, Z. Chai and X. Gao, *ACS Nano*, 2015, **9**, 4976–4986.
75 Y. F. Zhao, D. Sultan, L. Detering, S. H. Cho, G. R. Sun, R. Pierce, K. L. Wooley and Y. J. Liu, *Angew. Chem., Int. Ed.*, 2014, **53**, 156–159.
76 Y. F. Zhao, D. Sultan, L. Detering, H. Luehmann and Y. J. Liu, *Nanoscale*, 2014, **6**, 13501–13509.
77 H. Hu, P. Huang, O. J. Weiss, X. F. Yan, X. Y. Yue, M. G. Zhang, Y. X. Tang, L. M. Nie, Y. Ma, G. Niu, K. C. Wu and X. Y. Chen, *Biomaterials*, 2014, **35**, 9868–9876.
78 Y. Zhao, L. Detering, D. Sultan, M. L. Cooper, M. You, S. Cho, S. L. Meier, H. Luehmann, G. Sun, M. Rettig, F. Dehdashti, K. L. Wooley, J. F. DiPersio and Y. Liu, *ACS Nano*, 2016, **10**, 5959–5970.
79 T. Chen, Q. Yao, R. R. Nasaruddin and J. Xie, *Angew. Chem., Int. Ed.*, 2019, **58**, 11967–11977.
80 Q. Yao, X. Yuan, T. Chen, D. T. Leong and J. Xie, *Adv. Mater.*, 2018, **30**, 1802751.

81 P. Grodzinski, M. Kircher, M. Goldberg and A. Gabizon, *ACS Nano*, 2019, **13**, 7370–7376.
82 Y. Tao, Y. Lin, Z. Huang, J. Ren and X. Qu, *Adv. Mater.*, 2013, **25**, 2594–2599.
83 C. N. Loynachan, A. P. Soleimany, J. S. Dudani, Y. Lin, A. Najer, A. Bekdemir, Q. Chen, S. N. Bhatia and M. M. Stevens, *Nat. Nanotechnol.*, 2019, **14**, 883–890.
84 R. Liu, J. Zhai, L. Liu, Y. L. Wang, Y. T. Wei, X. L. Jiang, L. Gao, H. R. Zhu, Y. L. Zhao, Z. F. Chai and X. Y. Gao, *Chem. Commun.*, 2014, **50**, 3560–3563.
85 Q. Li, Q. Yuan, M. Zhao, Y. W. Yao, L. Gao, R. Liu, Y. L. Wang, Y. Gong, F. P. Gao and X. Y. Gao, *Sci. Bull.*, 2017, **62**, 537–545.
86 J. Zhai, Y. Jia, L. Zhao, Q. Yuan, F. Gao, X. Zhang, P. Cai, L. Gao, J. Guo, S. Yi, Z. Chai, Y. Zhao and X. Gao, *ACS Nano*, 2018, **12**, 4378–4386.
87 X.-D. Zhang, Z. Luo, J. Chen, S. Song, X. Yuan, X. Shen, H. Wang, Y. Sun, K. Gao, L. Zhang, S. Fan, D. T. Leong, M. Guo and J. Xie, *Sci. Rep.*, 2015, **5**, 8669.